

Mn²⁺-doped Fe₃O₄ nanoparticles: a novel preparation method, structural, magnetic and electrochemical characterizations

Mustafa Aghazadeh¹ · Isa Karimzadeh² · Mohammad Reza Ganjali^{3,4} · Ahmad Behzad¹

Received: 27 April 2017 / Accepted: 18 August 2017 / Published online: 21 August 2017
© Springer Science+Business Media, LLC 2017

Abstract A novel electrosynthesis procedure was applied to prepare manganese-doped iron oxide (Fe₃O₄) nanoparticles. The procedure involved depositing Fe₃O₄ nanoparticles on a steel cathode from aqueous solution of (2 g/L) Fe(NO₃)₃, (1 g/L) FeCl₂ and (0.3 g/L) MnCl₂. Next the product was evaluated using X-ray diffraction (XRD), field emission electron microscopy (FE-SEM) and energy-dispersive X-ray (EDX). The final optimal product was found to contain 10 wt% of Mn²⁺ and the average size of the spherical Mn-Fe₃O₄ nanoparticles was determined to be 20 nm. Further analysis of the produced particles using VSM proved it to have super-paramagnetic behavior ($M_s = 47.25 \text{ emu g}^{-1}$, $M_r = 0.22 \text{ emu g}^{-1}$, positive $M_r = -0.703 \text{ emu g}^{-1}$, negative $M_r = -1.15 \text{ emu g}^{-1}$, $H_{Ci} = 4.84 \text{ G}$, positive $H_{Ci} = 25.55$ and negative $H_{Ci} = 15.85 \text{ G}$). The nanoparticles were studied using electrochemical techniques of cyclic voltammetry, galvanostatic charge–discharge and electrochemical impedance spectroscopy, and it was found that the nanoparticles possess a specific capacitance value of 202.5 F g^{-1} , and capacity maintain about 92.4% after 2000 cycles at 0.5 A g^{-1} , which indicated the particles have excellent potential for use in supercapacitors.

1 Introduction

Supercapacitors (SCs), also known as electrochemical capacitors, are a new generation of energy storage systems, which offer high specific powers in the range of ~500–10,000 W/kg, and long cycle lives (>100,000 cycles). Such devices can find applications in mobile phones, electrical cars, memory devices and uninterruptible power supplies (UPSs) [1]. The electro-active materials used in supercapacitors plays a key role in their electrochemical behaviors and consequently developing cheap and suitable electrodes can be a huge step in the development and improvement of SCs. Hence, a great deal of works has been invested on preparing such electrode materials for SCs. As a result transition metal oxides and hydroxides with different structures (e.g. Co₃O₄ [2–4], CuO [5], NiO [6–10], MoO₃ [11], MnO₂ [12–19], Co(OH)₂ [20–28], Ni(OH)₂ [29–33], Fe₂O₃ [34–36] and Fe₃O₄ [37–40] wires, plates or sheets, spheres, rods, nanocapsules and worms) have been found as the proper compounds for use in the construction of supercapacitor electrodes. Iron oxides, as an instance of such materials, have been found to be very suitable due to the variable oxidation states of iron, its natural abundance, low cost, and environmental friendliness [41]. One drawback, in the case of iron compounds, which has limited their application in supercapacitors, is their limited SC values and charge/discharge rates which arise from their rather low conductivity [42, 43]. To solve this problem, several approaches including preparing iron oxide composites with carbon-based material (e.g. graphene, carbon nanotubes,...) [44–46], doping with other metal ions [47], and designing new nanostructures [48–51] have been evaluated, and the results revealed improved capacitances due to improvements such as enhanced conductivity, increased surface area, shortened diffusion paths and enhanced redox activity. Review of the literature reveals that

✉ Mustafa Aghazadeh
maghazadeh@aeoi.org.ir

¹ Materials and Nuclear Research School, Nuclear Science and Technology Research Institute (NSTRI), P. O. Box 14395-834, Tehran, Iran
² Department of Physics, Faculty of Science, Central Tehran Branch, Islamic Azad University, Tehran, Iran
³ Center of Excellence in Electrochemistry, Faculty of Chemistry, University of Tehran, Tehran, Iran
⁴ Biosensor Research Center, Endocrinology and Metabolism Molecular-Cellular Sciences Institute, Tehran University of Medical Sciences, Tehran, Iran

metal ion doping approach has not been intensively studied and hence the focus of this work was developing a novel method for preparing metal ion (i.e. Mn^{2+}) doped magnetite nanoparticles (MNPs) through an electrodeposition method. The recent work by our team on preparing pure magnetite nanoparticles through cathodic electrodeposition (CED) from iron (III) nitrate/iron(II) solutions without using any additives [52–55], gave our team the experience to evaluate a similar strategy for preparing Mn- Fe_3O_4 nanoparticles, which has not been reported in the literature so far.

2 Experimental procedure

2.1 Materials

Ferrous chloride tetrahydrate ($\text{FeCl}_2 \cdot 4\text{H}_2\text{O}$, 99.5%), ferric nitrate nonahydrate ($\text{Fe}(\text{NO}_3)_3 \cdot 9\text{H}_2\text{O}$, 99.9%), manganese chloride ($\text{MnCl}_2 \cdot 4\text{H}_2\text{O}$, 99.5%) and polyvinylidene fluoride (PVDF, $(\text{CH}_2\text{CF}_2)_n$) were purchased from Sigma Aldrich and used as received.

2.2 Electrosynthesis of Mn doped Fe_3O_4 nanoparticles

Previous reports on the application of cathodic electrodeposition (CED) for preparing naked and coated magnetite nanoparticles (MNPs) [55–57], were used as the basis for the preparation of Mn-doped Fe_3O_4 nanoparticles according to the schematic procedure in Fig. 1. To this end a $5\text{cm} \times 5\text{cm} \times 0.5\text{ mm}$ 316L stainless-steel element was used as the cathode. The cathode was sandwiched

between two parallel graphite pieces (anodes) and 1 L of aqueous solution containing 2 g of $\text{Fe}(\text{NO}_3)_3 \cdot 9\text{H}_2\text{O}$, 1 g of $\text{FeCl}_2 \cdot 4\text{H}_2\text{O}$ and 0.3 g of $\text{MnCl}_2 \cdot 4\text{H}_2\text{O}$ was used as the reaction solution. The deposition of product was performed using a NCF-PGS 2012 potentiostat/galvanostat workstation system (Iran) a current density of 10 mA cm^{-2} at $25\text{ }^\circ\text{C}$ for half an hour. Once the reaction was over, cathode was washed with deionized water, the solid deposit was scratched from its surface and repeatedly washed with water, and eventually dispersed in deionized water, centrifuged at 6000 rpm for 20 min, and eventually separated using a magnet, dried at $70\text{ }^\circ\text{C}$ for 60 min.

2.3 Characterization

An FE-SEM instrument (Mira 3-XMU, accelerating voltage of 100 kV) was used for studying morphology of the product. Also PW-1800 X-ray diffraction (XRD) with a $\text{Co K}\alpha$ radiation was used to study the crystal structure of the product. Thermogravimetric analyses of the sample were performed between room temperature and $600\text{ }^\circ\text{C}$ under an N_2 atmosphere and at a rate of $5\text{ }^\circ\text{C min}^{-1}$ using an STA-1500 Thermoanalyzer. Further the magnetic hysteresis and saturation magnetization studies were performed in the range of $-20,000$ to $20,000\text{ Oe}$ at ambient temperature using a vibrational sample magnetometer (VSM, Meghnatis Daghigh Kavir Co., Iran). The FTIR studies were performed on a Bruker Vector 22 instrument. Each spectrum was recorded by 20 scans in the range of $400\text{--}4000\text{ cm}^{-1}$ at a resolution of 4 cm^{-1} .

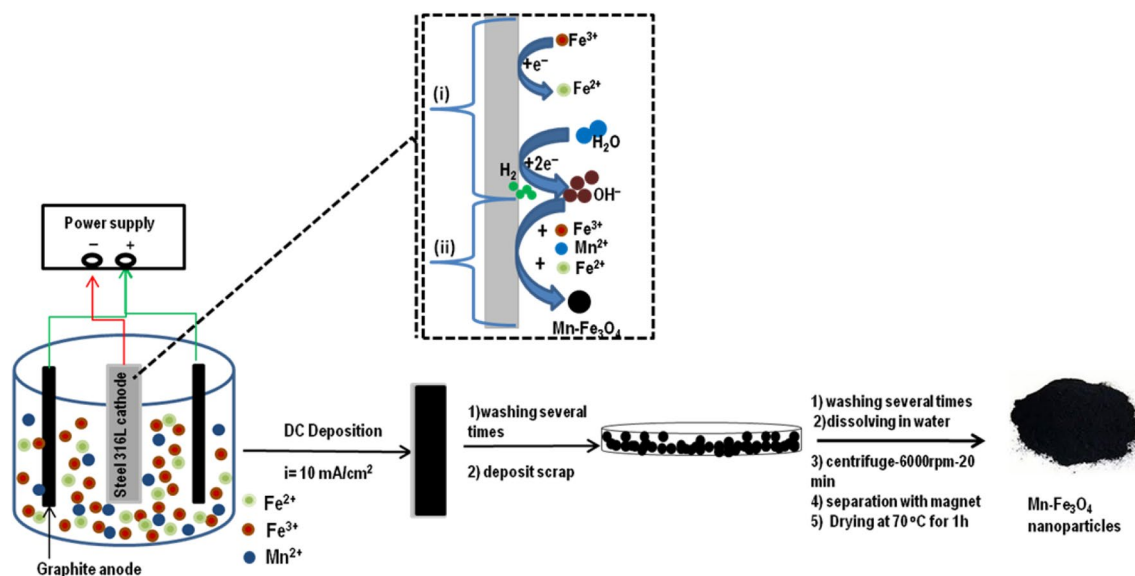


Fig. 1 Schematic view of electro-synthesis of Mn- Fe_3O_4 nanoparticles. The inset presents (i) electrochemical and (ii) chemical steps

2.4 Electrochemical characterization

An AUTOLAB®, Eco Chemie, PGSTAT 30 potentiostat was used for the cyclic voltammetry (CV) and galvanostatic charge–discharge (GCD) studies, which were performed using a three electrode system including a working electrode (WE) based on the Mn-Fe₃O₄ nanoparticles, a (1 M KCl) Ag/AgCl reference, and a platinum wire as the counter electrode, in the presence of a 1M Na₂SO₃ solution. The Mn-Fe₃O₄ WEs were prepared according to a well-established procedure [58, 59], based on which Mn-Fe₃O₄ powder, acetylene black (>99.9%) and conducting graphite (at wt% ratios of 75:10:10) were mixed and homogenized. Then, 5 wt% of polyvinylidene fluoride (PVDF) was added to this mixture as dissolved in N-Methyl-2-pyrrolidone (NMP). Then the NMP present in the mixture was partially evaporated and a mass of the paste containing 3 mg of the synthesized nanoparticles was pressed onto a 1 cm² Ni foam at 10 MPa. The assembly was then dried at 150 °C in oven for 5 min.

CV studies were performed using these WEs, in a 1M Na₂SO₃ solution over a potential window of -1.0 and +0.1 V versus Ag/AgCl, at the scan rates of 2, 5, 10, 20, 50 and 100 mV s⁻¹. The resulting data was used for calculating the SC of the electroactive material using Eq. (1) [12]:

$$SC = \frac{Q}{m\Delta V}, \quad Q = \int_{V_a}^{V_b} I(V)dV \tag{1}$$

where SC is specific capacitance (F g⁻¹), Q represents the total charge, ΔV represents the potential, m is the mass of the electroactive material (i.e. Mn-Fe₃O₄ powder (g), v is the scan rate (V s⁻¹) and I(V) is the current response.

GCD plots were obtained at the current loads of 0.5, 1, 2, 3 and 5 A g⁻¹ in the voltage range of -1.0 to 0V versus Ag/AgCl, and the results were translated into SC values using the following equation [39]:

$$SC = \frac{Q}{m \times \Delta V}, \quad Q = I \times \Delta t \tag{2}$$

in which, I and ΔV are the applied current load (A) and potential range (1V), Δt is the duration of a discharge cycle (s) and m represents the mass of the electroactive material (g). The EIS studies were performed at the open circuit potential in a AC frequencies ranging from 10⁵ to 10⁻² Hz and at an excitation signal of 5 mV.

3 Results and discussion

3.1 Structure and morphology

The XRD pattern of our sample (Fig. 2) included all diffraction peaks observed in the case of pure cubic phase

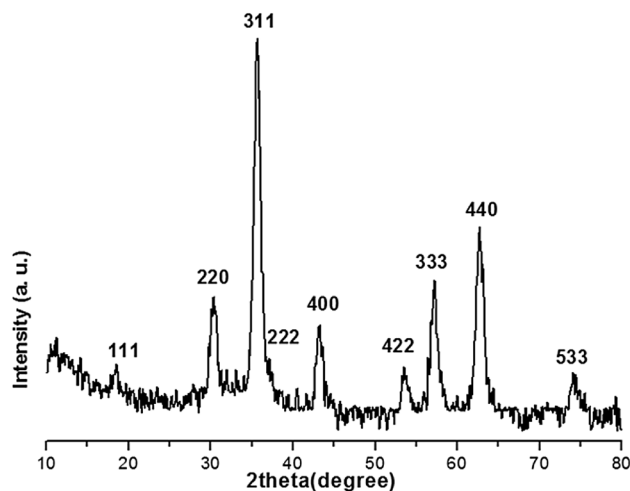


Fig. 2 XRD pattern of the electro-synthesized Mn doped Fe₃O₄ nanoparticles

[space group: Fd3m (227)] Fe₃O₄ (cell constant of a = 8.389 Å, JCPDS 01-074-1910).

In this pattern, no extra peaks were observed proving the pure phase of product, and it was established Mn²⁺ acts similar to Fe²⁺ ions at the deposition and formation steps. The average crystallite size (D) of the product was determined through the Debye–Scherrer equation:

$$D = 0.9\lambda / \beta \cos(\theta)$$

In this equation, λ is the X-ray wavelength, β represents the full width at the half maximum of the diffraction line, and θ is the diffraction angle. Based on the calculations using diffraction line-width of peak (311), D value was determined to be 12.8 nm.

Surface morphology studies were also conducted through FE-SEM and the results (Fig. 3a) clearly show that the sample was composed of particles with an average diameter of about 20 nm. The results of elemental analyses of the sample based on energy-dispersive X-ray (EDX) (Fig. 3b) reveals that the NPs contain Fe, Mn and O elements in the mass percentages of 63.36, 9.71 and 26.93, respectively. Considering that, based on the XRD data, some of Fe²⁺ ions have been substituted with Mn²⁺, the values are very close to the composition of Fe₃O₄ in terms of Fe and O (27.64% for O and 72.36% for Fe). Based on the results the sample was determined to be 10 wt% Mn²⁺ doped Fe₃O₄.

The FT-IR spectrum of the sample (Fig. 4a) contains the characteristic bands of nano-sized magnetite [60–62]. These include two sharp bands at about 567 and 628 cm⁻¹, due to the splitting of the ν₁ band of the Fe–O, and a wide one at 435 cm⁻¹ due to the ν₂ band of the Fe–O and/or Mn–O bonds [61]. The FT-IR data also showed bands around 1635 and 3441 cm⁻¹ due to the stretching and deformation vibrations of the surface absorbed O–H

Fig. 3 **a** FE-SEM image and **b** EDAX analysis of the prepared Mn doped Fe_3O_4 nanoparticles

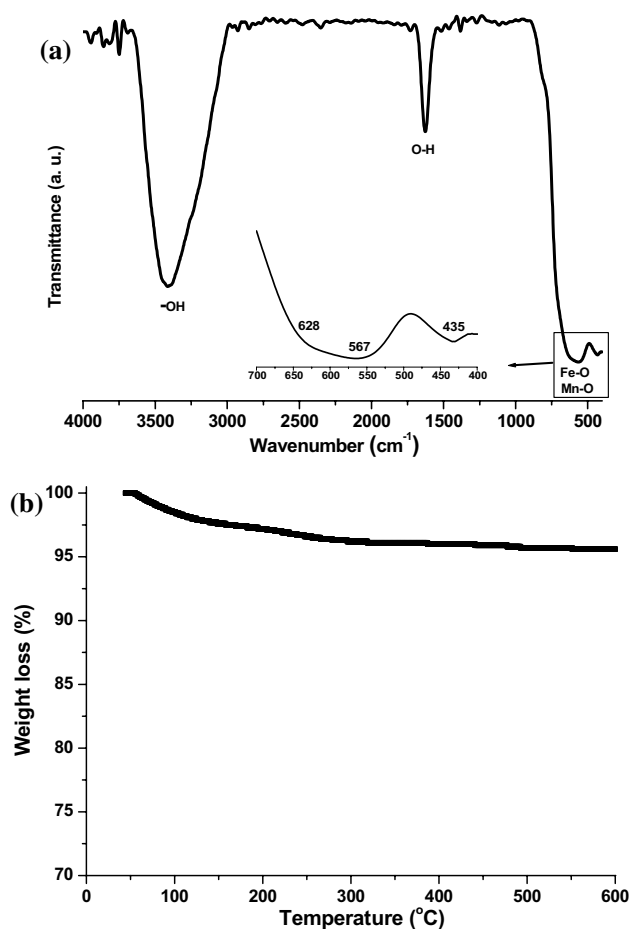
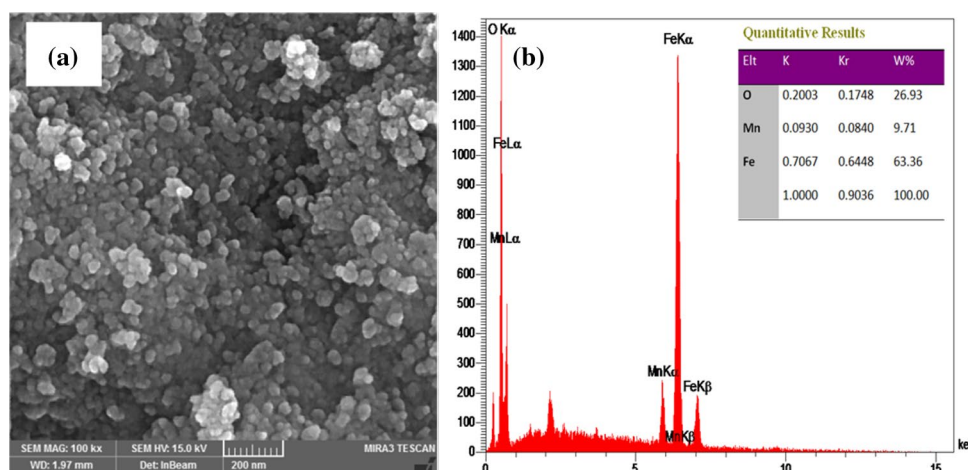


Fig. 4 **a** IR spectrum and **b** TG curve of the electrodeposited Mn doped Fe_3O_4 nanoparticles

groups and H_2O [62], which further complies with the XRD results (Fig. 2).

The thermo-gravimetric (TG) behavior of the sample obtained in the range of 25–700 °C (Fig. 4b) indicated no sharp weight loss peak proving the stability of the sample.

The mere 3.8% weight loss below 200 °C, was attributed to the elimination of the surface absorbed H_2O molecules, and the overall the TG profile of the sample was quiet similar to those observed in the case of pure magnetite NPs reported in other articles [61, 62].

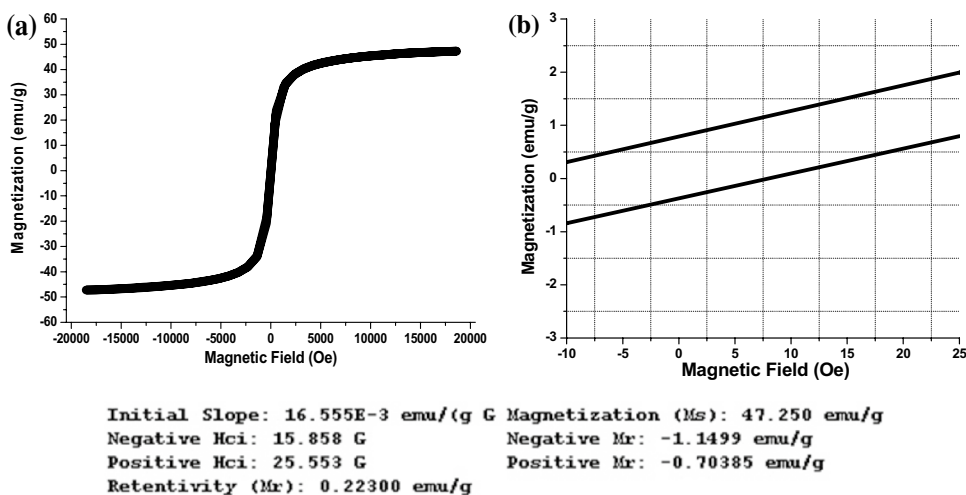
Figure 5 illustrates the magnetic hysteresis loop and the enlarged low-field hysteresis. The VSM plot in Fig. 5a has a complete S shape and no hysteresis can be noticed (Fig. 5b), indicating the superparamagnetic nature of the product. Further magnetic data obtained for the sample included the saturation magnetization (M_s), remanent magnetization or retentivity (M_r) and coercivity (H_{Ci}), which are $M_s = 47.25 \text{ emu g}^{-1}$, $M_r = 0.22 \text{ emu g}^{-1}$, positive $M_r = -0.703 \text{ emu g}^{-1}$, negative $M_r = -1.15 \text{ emu g}^{-1}$, $H_{Ci} = 4.84 \text{ G}$, positive $H_{Ci} = 25.55$ and negative $H_{Ci} = 15.85 \text{ G}$. These data further confirmed the superparamagnetic behavior of the sample. The data were also comparable with those of naked pure Fe_3O_4 NPs electro-synthesized under similar conditions as the sample. Comparison against magnetic data on pure Fe_3O_4 NPs reported in other works [61, 62] (*i.e.* $M_s = 72.96 \text{ emu g}^{-1}$, $M_r = 0.95 \text{ emu g}^{-1}$, positive $M_r = 2.73 \text{ emu g}^{-1}$, negative $M_r = -0.83 \text{ emu g}^{-1}$, $H_{Ci} = 14.61 \text{ G}$, positive $H_{Ci} = -12.66$ and negative $H_{Ci} = -41.88 \text{ G}$) proved that the Mn-doped Fe_3O_4 NPs have rather lower saturation magnetization due, most probably, to the low magnetic nature of Mn^{2+} ions. Yet the doped sample has smaller M_r and H_{Ci} as opposed to pure Fe_3O_4 NPs, which proved their enhanced superparamagnetic behavior.

3.2 Electrochemical assessments

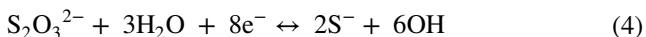
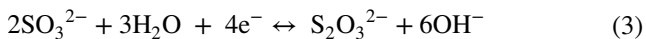
3.2.1 Cyclic voltammetry

The SC of the electroactive materials used in constructing the WEs was evaluated through CV, and GCD tests. Further EIS studies were performed to evaluate the electrochemical

Fig. 5 **a** Hysteresis curve of Mn-Fe₃O₄ NPs and **b** its enlarged low-field region



properties of the sample as electrode material. The CVs in Fig. 6a were obtained in the above-described three-electrode system at 2, 5, 10, 20, 50 and 100 mV s⁻¹, over potential window of -1.0 to 0.1 V versus Ag/AgCl. The form of the CVs indicates the pseudo-capacitive nature of the electroactive material, which is different from the electric double-layer capacitance mechanism. It has formerly been reported that the charge storage of Fe₃O₄ based electrodes in Na₂SO₃ solution takes place through a combination of both EDLC and pseudocapacitance mechanisms. The latter is known to involve the reduction/oxidation of the adsorbed sulfite anions preset on the surface of iron oxide particles [38, 39]. The CVs in Fig. 5 include small humps, which can be attributed to the redox reactions of the surface adsorbed sulfite anions [41, 63]:



No shifts were observed in the position of the anodic and cathodic peaks, which indicate the reversibility and continuous nature of the redox reactions [43, 63]. The specific capacitances of our electroactive, using Eq. (1), were found to be 242.1, 225.4, 199.7, 163.2, 134.5, 95.9 and 80.7 F g⁻¹

at 1, 2, 5, 10, 20, 50 and 100 mV s⁻¹, respectively, further confirming the excellent super-capacitive behavior of the particles.

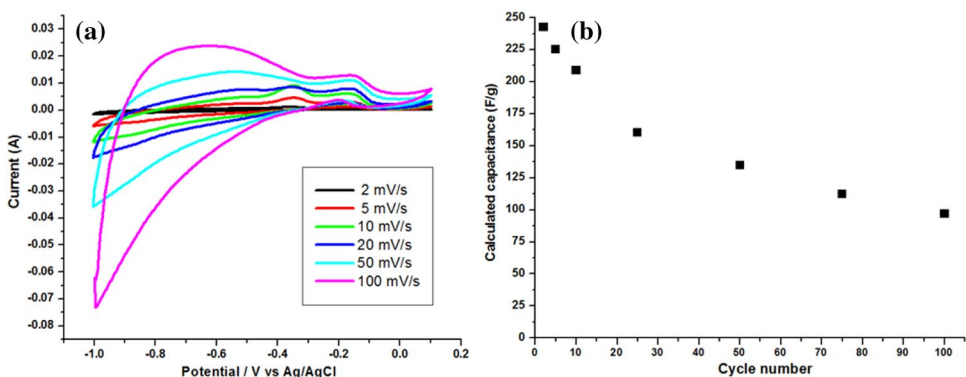
3.2.2 Charge–discharge tests

The galvanostatic charge–discharge (GCD) plots recorded at 0.5, 1, 2, 3 and 5 A g⁻¹, as given in Fig. 6a. The GCD profile of the fabricated WE can be divided into parts; first a symmetric triangular section below -0.5 V versus Ag/AgCl, and a nonlinear part over this potential. The former confirms the pure double-layer capacitance due to the charge separation phenomenon at the electrode–electrolyte interface, while the latter is indicative of a typical pseudo-capacitance behavior (Eqs. 3 and 4). The SC values of the product was calculated using Eq. (2), based on the data.

The calculations showed that the doped Fe₃O₄ nanoparticles offer SC values of 202.8 F g⁻¹ at 0.5 A g⁻¹, 176.5 F g⁻¹ at 1 A g⁻¹, 141.2 F g⁻¹ at 2 A g⁻¹, 123.3 F g⁻¹ at 3 A g⁻¹ and 102.4 F g⁻¹ at 5 A g⁻¹, which comply with the results obtained from the CVs (Fig. 6b).

The charge storage behavior of the Mn-Fe₃O₄ nanoparticles was also found to be comparable with those of pure

Fig. 6 **a** CVs of the fabricated Mn doped Fe₃O₄ electrode at 2 mV/s and **b** at the various scan rates, **c** the calculated specific capacitances versus scan rate



Fe_3O_4 electrodes prepared through various methods; e.g. 185 F g^{-1} at 20 mV s^{-1} for Fe_3O_4 (synthesized by sol–gel) [37], 207 F g^{-1} for Fe_3O_4 at 0.4 A g^{-1} (prepared from ultrasonic synthesis) [39], 157 F g^{-1} at 1 A g^{-1} for Fe_3O_4 (obtained by PVP-assisted hydrothermal method) [63], 170 F g^{-1} at 2 mV s^{-1} for Fe_3O_4 thin film (prepared by electroplating) [64], 118.2 F g^{-1} at 0.6 A g^{-1} for Fe_3O_4 thin film (fabricated using hydrothermal method) [65] and 82 F g^{-1} at 1 A g^{-1} for Fe_3O_4 thin film (deposited by co-precipitation method) [66]. Comparing the data proved that the supercapacitive performance Fe_3O_4 can be enhanced through doping with Mn^{2+} cations.

The cycling stability of electrode material was evaluated through subjecting the electrodes to 2000 GCD cycles in a $1 \text{ M Na}_2\text{SO}_3$ solution at two current densities of 0.5 and 2 A/g . The SCs of each cycle were calculated using Eq. (2), and the results showed the cycling stability of the nanoparticles. The SCs and cycling stabilities of the electrode material are presented in Fig. 7b, c. According to Fig. 7b, the SC of the electroactive material decreased from 202.8 to 187.4 F g^{-1} after 2000 cycles at 0.5 A g^{-1} , which is

equivalent to maintaining about 92.4% of the initial SC (Fig. 7c). At 2 A g^{-1} , the SC showed a decrease of about 83.5% after 2000 GCD cycles and reduced from 141.2 to 117.9 F g^{-1} . The data indicated the good cycling ability of the electrode material.

3.2.3 EIS measurement

Using results of EIS studies on the electrode material as Nyquist plots (Fig. 8), and the inset of Fig. 8 which magnifies the high frequency region of both plots, it can be said that the starting cross-point at the Z' axis within the high frequency region, shows the contact resistance (R_s) among the electrolyte/electrode, current collectors and electrode/current collector. Further the diameter of the semicircular section in the mid–frequency gives the charge-transfer resistance (R_{ct}) [46] and the straight line with a 45° slope in the low frequency region shows semi-infinite Warburg impedance (Z_w) [48, 49]. Both plots (in Fig. 8) have a linear section as well as a semicircular one and fits to that of an equivalent circuit composed of an electrolytic resistance (R_s), a double

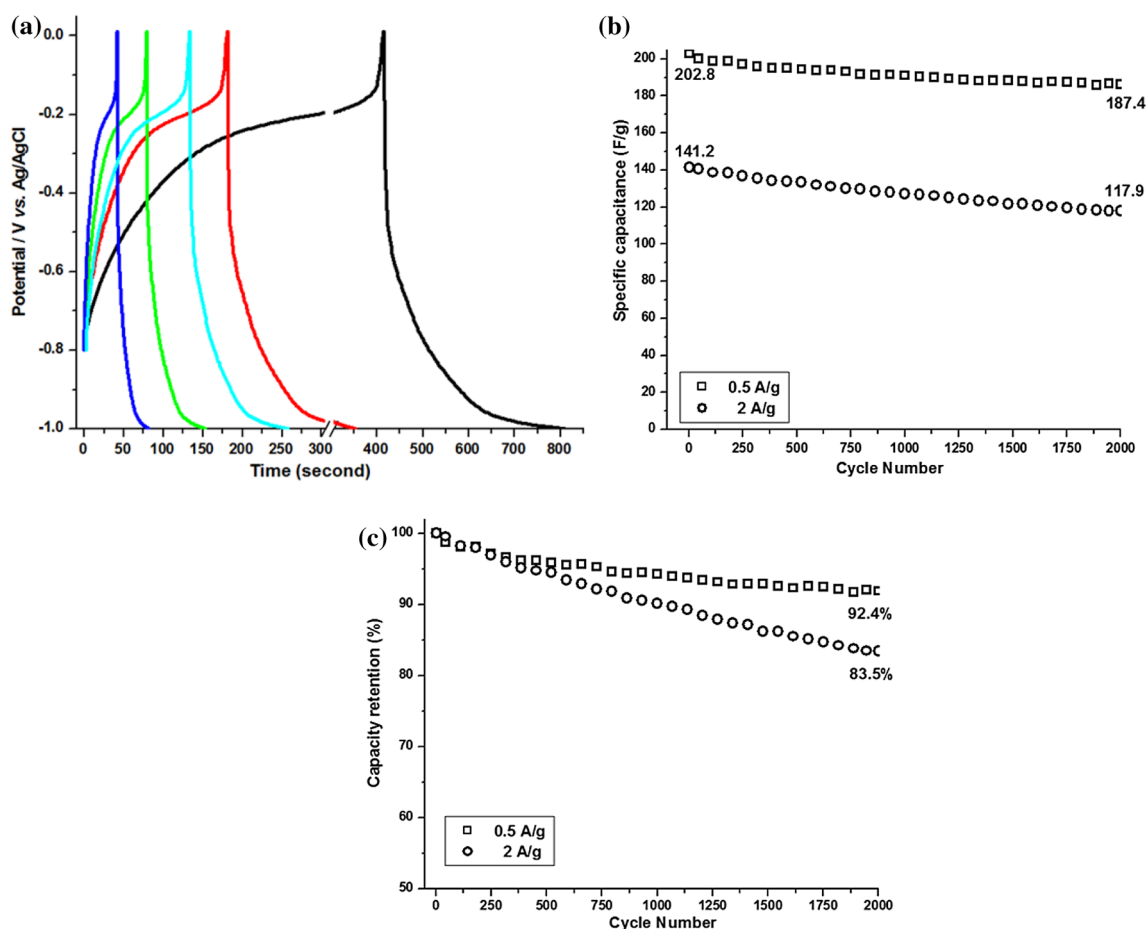


Fig. 7 **a** GCD profiles of the fabricated electrode and **b** specific capacitances and **c** capacity retentions during 2000 GCD cycling at the current loads of 0.5 and 2 A g^{-1}

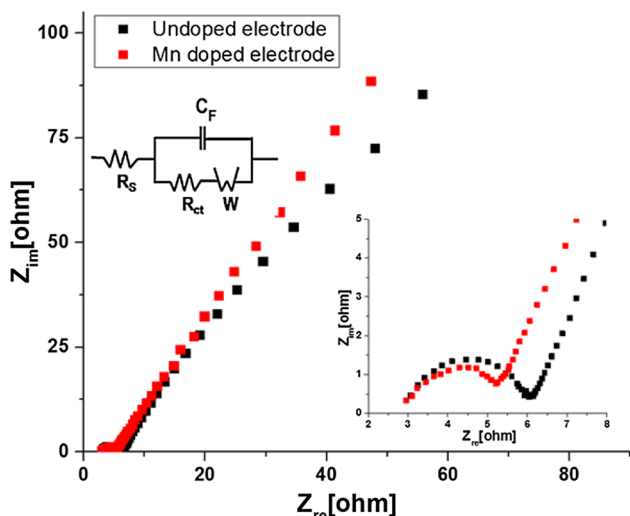


Fig. 8 Nyquist plots of undoped and Mn doped Fe₃O₄ electrodes with suggested equivalent circuit model

layer capacitor (C_{dl}), a charge transfer resistance (R_{ct}), a Warburg element (Z_w) and a pseudocapacitor (C_p) (as shown in inset of Fig. 8). Based on the Nyquist plots, R_{ct} values of undoped and Mn²⁺ doped electrodes were determined to be 3.25 and 2.05 Ω, respectively. Furthermore, from fitting data, it was obtained that the overall resistance of undoped and doped electrodes are 314 and 237 Ω, respectively. These results indicated the effectiveness of the electronic and ionic transfer at electrolyte/doped electrode interface and implicated its better reaction kinetic as compared with undoped electrode. Based on this curves, the R_s values of undoped and doped electrodes were found to be 2.81 and 3.05 Ω, respectively. These values indicated the small resistance and good ion response which are the results of the high purity, metal ion doping and excellent crystallinity of the material.

3.2.4 Optical properties analysis

UV–Vis absorption spectra of the prepared samples were measured to evaluate Mn-doping effect on Fe₃O₄ NPs optical properties such as optical absorption and band gap (Fig. 9). Having added 10 wt% Mn doping, sharp absorption edges appear in this region due to light absorption and scattering by nano-particles. For undoped Fe₃O₄ NPs, there is no sharp absorption edge in UV region. For Mn²⁺ doped MNPs, one optical absorption peak is clearly observed, which reflects Mn²⁺ incorporation into Fe₃O₄ lattice. Indirect band gap of doped MNPs was calculated by following equation [67]:

$$\alpha h\nu = A(h\nu - E_g)^2 \tag{5}$$

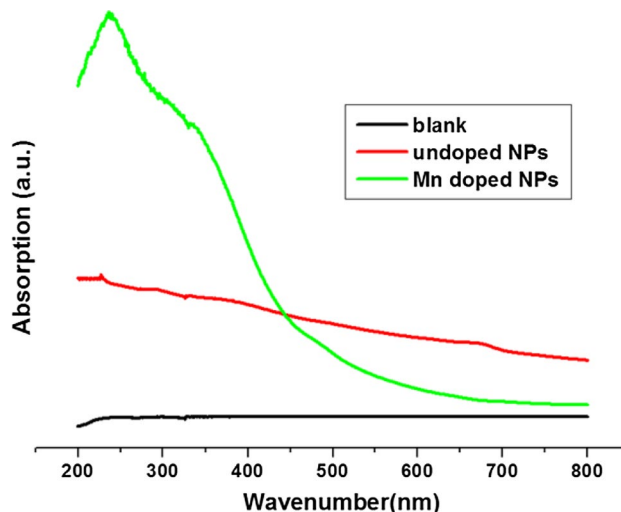


Fig. 9 UV–Vis absorption spectra of undoped and Mn²⁺ doped Fe₃O₄ nanoparticles

where α is the absorption coefficient, A is a constant, h is Planck’s constant, ν is the photon frequency and E_g is the energy [67]. In Eq. (5); when $\alpha h\nu = 0$, $h\nu = E_g$. Hence, E_g value can be determined through plotting a diagram of $(\alpha h\nu)^{1/2}$ versus $h\nu$ and then extrapolating its linear region [67, 68]. For our samples, plotting $(\alpha h\nu)^{1/2}$ versus $h\nu$ and then extrapolating gives E_g values of 0.12 and 1.96 eV for undoped and Mn²⁺ doped MNPs, respectively. These values indicate that E_g value in Mn-doped Fe₃O₄ NPs is higher that of pure Fe₃O₄ NPs. This can be ascribed to the fact that new defect are introduced after replacement of Fe²⁺ by Mn²⁺ cations in order to electro-negativity and ionic radius difference between Mn²⁺ and Fe²⁺. Moreover, there are more electrons contributed by Mn²⁺ dopant due to lower electron affinity of Mn compared to Fe (i.e. Mn = 0 KJ/mol⁻¹, Fe = 15 KJ/mol⁻¹) which take up the energy levels location in the bottom of the conduction band. The valence electrons require extra energy to be excited to higher energy states in the conduction band.

4 Conclusion

Mn-doped Fe₃O₄ particles (size ≈ 20 nm) were prepared through a one-pot electrochemical method under a galvanostatic mode. The deposition was performed in a solution of iron chloride/nitrate and manganese chloride, and the product was electrochemically deposited on the surface of a stainless steel cathode. The resulting material was found to have good capacitive ability with exhibiting SC values of 242.1, 225.4, 199.7, 163.2, 134.5, 95.9 and 80.7 F g⁻¹ at 1, 2, 5, 10, 20, 50 and 100 mV s⁻¹, respectively. The result of VSM analyses further confirmed the material to be

superparamagnetic in nature. In the light of the observations, the developed super material was suggested as a suitable material for the super-capacitor applications, and its preparation method was also found to be a promising approach for the preparation of nano-sized metal-doped iron oxides.

Compliance with ethical standards

Conflict of interest The authors declare that there is no conflict of interest about publishing this paper.

References

- P. Simon, Y. Gogotsi, *Nat. Mater.* **7**, 845 (2008)
- M. Aghazadeh, R. Ahmadi, D. Gharailou, M.R. Ganjali, P. Norouzi, *J. Mater. Sci.* **27**, 8623 (2016)
- M. Aghazadeh, *J. Appl. Electrochem.* **42**, 89 (2012)
- M. Aghazadeh, A. Rashidy, P. Norouzi, *Int. J. Electrochem. Sci.* **11**, 11016 (2016)
- Q. Chunling, Z. Yanshan, W. Zhifeng, X. Hanqing, Y. Hui, Z. Weimin, *J. Mater. Sci.* **9**, 9206 (2016)
- M. Aghazadeh, M.R. Ganjali, *J. Mater. Sci.* **28**, 8144 (2017)
- M. Aghazadeh, A. Rashidi, M.R. Ganjali, *Int. J. Electrochem. Sci.* **11**, 11002 (2016)
- M. Aghazadeh, *J. Mater. Sci.* **28**, 3108 (2017)
- A. Barani, M. Aghazadeh, M.R. Ganjali, B. Sabour, A.A.M. Barmi, S. Dalvand, *Mater. Sci. Semiconduct. Process* **23**, 85 (2014)
- H.M. Shiri, M. Aghazadeh, *J. Electrochem. Soc.* **159**, E132 (2012)
- S. Ramya, G. Viruthagiri, R. Gobi, N. Shanmugam, N. Kannadasan, *J. Mater. Sci.* **27**, 2701 (2016)
- R. Poonguzhali, N. Shanmugam, R. Gobi, A. Senthilkumar, G. Viruthagiri, N. Kannadasan, *J. Power Sources* **293**, 790 (2015)
- M. Aghazadeh, A. Bahrami-Samani, D. Gharailou, M. Ghannadi Maragheh, M.R. Ganjali, *J. Mater. Sci.* **27**, 11192 (2016)
- M. Aghazadeh, M.R. Ganjali, P. Norouzi, *J. Mater. Sci.* **27**, 7707 (2016)
- J. Tizfahm, M. Aghazadeh, M.G. Maragheh, M.R. Ganjali, P. Norouzi, *Mater. Lett.* **167**, 153 (2016)
- M. Aghazadeh, M.G. Maragheh, M.R. Ganjali, P. Norouzi, D. Gharailou, F. Faridbod, *J. Mater. Sci.* **27**, 7707 (2016)
- M. Aghazadeh, M. Asadi, M.G. Maragheh, M.R. Ganjali, P. Norouzi, *Appl. Surf. Sci.* **364**, 726 (2016)
- M. Aghazadeh, M.G. Maragheh, M.R. Ganjali, P. Norouzi, F. Faridbod, *Appl. Surf. Sci.* **364**, 141 (2016)
- M. Aghazadeh, M.R. Ganjali, P. Norouzi, *Thin Solid Films* **634**, 24 (2017)
- L. He-Ming, Z. Feng-Bo, Z. Xia, Z. De-Yi, W. Yan-Xia, P.Y. Sun, *J. Mater. Sci.* **7**, 2473 (2013)
- M. Aghazadeh, A.A. Malek Barmi, D. Gharailou, M.H. Peyrovi, B. Sabour, F. Najafi, *Appl. Surf. Sci.* **283**, 871 (2013)
- G.H. Jeong, H.M. Lee, H. Lee, C.K. Kim, Y. Piao, J.H. Lee, J.H. Kim, S.W. Kim, *RSC Adv.* **4**, 51619 (2014)
- M. Aghazadeh, S. Dalvand, *J. Electrochem. Soc.* **161**, D18 (2014)
- M. Aghazadeh, S. Dalvand, M. Hosseinifard, *Ceram. Int.* **40**, 3485 (2014)
- M. Aghazadeh, H. Mohammad Shiri, A.A. Malek Barmi, *Appl. Surf. Sci.* **273**, 237 (2013)
- M. Aghazadeh, M.R. Ganjali, *J. Mater. Sci.* **28**, 11406 (2017)
- J. TalatMehrabad, M. Aghazadeh, M. Ghannadi Maragheh, M.R. Ganjali, *Mater. Lett.* **184**, 223 (2016)
- M. Aghazadeh, M.R. Ganjali, M.G. Maragheh, *Int. Electrochem. Sci.* **12**, 5792 (2017)
- J. Gou, S. Xie, Y. Liu, C. Liu, *Electrochim. Acta* **210**, 915 (2016)
- J. Tizfahm, B. Safibonab, M. Aghazadeh, A. Majdabadi, B. Sabour, S. Dalvand, *Colloids Surf. A* **443**, 544 (2014)
- M. Aghazadeh, A. Nozad Golikand, M. Ghaemi, *Int. J. Hydrog. Energy* **36**, 8674 (2011)
- M. Aghazadeh, M. Ghaemi, B. Sabour, S. Dalvand, *J. Solid State Electrochem.* **18**, 1569 (2014)
- M. Aghazadeh, B. Sabour, M.R. Ganjali, S. Dalvand, *Appl. Surf. Sci.* **313**, 581 (2014)
- A.A. Yadav, *J. Mater. Sci.* **27**, 12876 (2016)
- H. Gholipour-Ranjbar, M.R. Ganjali, P. Norouzi, H.R. Naderi, *Ceram. Int.* **42**, 12097 (2016)
- M. Aghazadeh, I. Karimzadeh, M.R. Ganjali, *J. Mater. Sci.* (2017). doi:10.1007/s10854-017-7192-z
- E. Mitchell, R.K. Gupta, K. Mensah-Darkw, D. Kumar, K. Ramasamy, B.K. Gupta, P. Kahol, *New J. Chem.* **38**, 4344 (2014)
- V.D. Nithya, N. Sabari Arul, *J. Power Source* **327**, 297 (2016)
- L. Wang, H. Ji, S. Wang, L. Kong, X. Jiang, G. Yang, *Nanoscale* **5**, 3793 (2013)
- M. Aghazadeh, I. Karimzadeh, M.R. Ganjali, *Mater. Lett.* **196**, 392 (2017)
- V.D. Nithya, N. Sabari Arul, *J. Mater. Chem. A* **4**, 10767 (2016)
- Z. Zhou, W. Xie, S. Li, X. Jiang, D. He, S. Peng, F. Ma, *J. Solid State Electrochem.* **19**, 1211 (2015)
- Y. Yang, J. Li, D. Chen, J. Zhao, *ACS Appl. Mater. Interfaces* **8**, 26730 (2016)
- S. Chen, R. Zhou, Y. Chen, Y. Fu, P. Li, Y. Song, L. Wang, *J. Nanopart. Res.* **19**, 127 (2017)
- Y.Z. Wu, M. Chen, X.H. Yan, J. Ren, Y. Dai, J.J. Wang, J.M. Pan, Y.P. Wang, X.N. Cheng, *Mater. Lett.* **198**, 114 (2017)
- H. Fan, R. Niu, J. Duan, W. Liu, W. Shen, *ACS Appl. Mater. Interfaces* **8**, 19475 (2016)
- X. Yang, J. Kan, F. Zhang, M. Zhu, Z. Li, *J. Inorg. Org. Polym. Mater.* **27**, 542 (2017)
- X. Tang, R. Jia, T. Zhai, H. Xia, *ACS Appl. Mater. Interfaces* **7**, 27518 (2015)
- T. Xia, X. Xu, J. Wang, C. Xu, F. Meng, Z. Shi, J. Lian, J.M. Basat, *Electrochim. Acta* **160**, 114 (2015)
- W.M. Zhang, X.L. Wu, J.S. Hu, Y.G. Guo, L.J. Wan, *Adv. Funct. Mater.* **18**, 3941 (2008)
- X. Xia, Y. Zhang, D. Chao, C. Guan, Y. Zhang, L. Li, X. Ge, I. Minguez, J. Bacho, Tu, H.J. Fan, *Nanoscale* **6**, 5008 (2014)
- I. Karimzadeh, M. Aghazadeh, M.R. Ganjali, P. Norouzi, T. Doroudi, *Mater. Lett.* **189**, 290 (2017)
- I. Karimzadeh, H. Rezagholipour Dizaji, M. Aghazadeh, *Mater. Res. Exp.* **3**, 095022 (2016)
- I. Karimzadeh, M. Aghazadeh, M.R. Ganjali, P. Norouzi, S. Shirvani-Arani, *Mater. Lett.* **179**, 5 (2016)
- I. Karimzadeh, M. Aghazadeh, M.R. Ganjali, T. Dourudi, *Curr. Nanosci.* **13**, 167 (2017)
- I. Karimzadeh, M. Aghazadeh, T. Doroudi, M.R. Ganjali, P.H. Kolivand, *Adv. Phys. Chem.* **2017**, 7 (2017)
- I. Karimzadeh, M. Aghazadeh, T. Doroudi, M.R. Ganjali, D. Gharailou, *J. Cluster Sci.* **12**, 3231 (2017)
- L.G. Beka, X. Li, W. Liu, *J. Mater. Sci.* **27**, 10894 (2016)
- P. Razmjoo, B. Sabour, S. Dalvand, M. Aghazadeh, M.R. Ganjali, *J. Electrochem. Soc.* **161**, D293 (2014)
- M. Aghazadeh, I. Karimzadeh, T. Doroudi, M.R. Ganjali, P.H. Kolivand, D. Gharailou, *Curr. Nanosci.* **13**, 274 (2017)
- I. Karimzadeh, M. Aghazadeh, M.R. Ganjali, P. Norouzi, D. Gharailou, *Mater. Lett.* **179**, 5 (2016)
- M. Aghazadeh, I. Karimzadeh, M.R. Ganjali, M. Mohebi Morad, *Mater. Lett.* **196**, 392 (2017)
- K. Bhattacharya, P. Deb, *Dalton Trans.* **44**, 9221 (2015)

64. S.Y. Wang, K.C. Ho, S.L. Kuo, N.L. Wu, *J. Electrochem. Soc.* **153**, A75 (2006)
65. J. Chen, K. Huang, S. Liu, *Electrochim. Acta* **55**, 1 (2009)
66. S.C. Pang, W.H. Khoh, S.F. Chin, *J. Mater. Sci.* **45**, 5598 (2010)
67. J. Guo, Y. Sun, B. Liu, Q. Zhang, Q. Peng, *J. Alloys Compd.* **712**, 752 (2017)
68. N.R. Ramanujam, K.S. Joseph, Wilson, *Optics Commun.* **368**, 174 (2016)